X-682-73-210
PREPRINT

NASA TM X- 66299

SPATIAL DISTRIBUTION OF SOFT X-RAY AND EUV EMISSION ASSOCIATED WITH A CHROMOSPHERIC FLARE OF IMPORTANCE 1B ON AUGUST 2, 1972

(NASA-TM-X-66299) SPATIAL DISTRIBUTION OF SOFT X-RAY AND EUV EMISSION ASSOCIATED WITH A CHROMOSPHERIC FLARE OF IMPORTANCE 1B ON 2 AUGUST 1972 (NASA) 56 p HC $5.00 N73-27720
Unclas
G3/29 09911

W. M. NEUPERT
R. J. THOMAS
R. D. CHAPMAN

AUG 1973
RECEIVED
NASA STI FACILITY
INPUT BRANCH

JULY 1973

GSFC
GODDARD SPACE FLIGHT CENTER
GREENBELT, MARYLAND

X-682-73-210

SPATIAL DISTRIBUTION OF SOFT X-RAY AND EUV EMISSION ASSOCIATED WITH A CHROMOSPHERIC FLARE OF IMPORTANCE 1B ON AUGUST 2, 1972

W. M. Neupert
R. J. Thomas
R. D. Chapman

July 1973

GODDARD SPACE FLIGHT CENTER
Greenbelt, Maryland

SPATIAL DISTRIBUTION OF SOFT X-RAY AND EUV EMISSION ASSOCIATED WITH A CHROMOSPHERIC FLARE OF IMPORTANCE 1B ON AUGUST 2, 1972

W. M. Neupert, R. J. Thomas and R. D. Chapman

Laboratory for Solar Physics
NASA-Goddard Space Flight Center
Greenbelt, Maryland 20771

Abstract

Soft X-ray and extreme ultraviolet spectroheliographs carried by the OSO-7 (Orbiting Solar Observatory) have been used to record the development of XUV emission associated with a flare of Importance 1B on August 2, 1972. Spatial resolution was 20 arc sec and spectral resolution was adequate to select emission lines originating within well-defined ranges of electron temperature between 0.05×10^6 and 30×10^6 K. The data show that heating only the pre-existing coronal material adjacent to the flare site cannot account for the soft X-ray emission measure observed during the event. The flare emission originating at $T_e \leq 2.3 \times 10^6$ K exhibits an impulsive component coincident with an impulsive microwave event. This radiation appears to coincide spatially with Hα radiation emitted at that time and is centered on the neutral line separating magnetic fields of opposite polarity. One soft X-ray-emitting feature, estimated to have an initial electron temperature of $2 - 10 \times 10^6$ K, forms during the impulsive phase immediately over the Hα flare. A second, arch-like feature observed at wavelengths near 1.9Å and estimated to have $T_e \cong 30 \times 10^6$ K is located approximately 35,000 km above the Hα event. Both regions have lengths of about

27,000 km but transverse dimensions small compared to the spatial resolution of the spectroheliograph, i.e., less than 14,000 km. The region with highest electron temperature exhibits the greatest stability in position. This region cools to approximately 10×10^6 K in 6 to 12 minutes which is compatible with cooling by conduction to the chromosphere. The best association with a dark surge is found in an emission line of Fe XIV.

SPATIAL DISTRIBUTION OF SOFT X-RAY AND EUV EMISSION ASSOCIATED WITH A CHROMOSPHERIC FLARE OF IMPORTANCE 1B ON AUGUST 2, 1972

W. M. Neupert, R. J. Thomas and R. D. Chapman

Laboratory for Solar Physics
NASA-Goddard Space Flight Center
Greenbelt, Maryland 20771

1. Introduction

Observations from above the earth's atmosphere by means of balloons, rockets and satellites provide the only means for observing directly the presence of the hot ($T_e > 5 \times 10^6$ K) quasi-thermal plasma frequently associated with solar flares. Early observations with broad-band detectors demonstrated not only the existence of short-lived X-ray enhancements in active regions (OSO-4 data reported by Vaiana and Giacconi, 1969) but also suggested that such enhancements may even occur in coronal regions not associated with active centers (Zhitnik, Krutov, Maljavkin, Mandelstam and Cheremukhin, 1967). Unfortunately these early observations had inadequate spatial resolution (of the order of 1-2 arc min) to provide meaningful information on the shapes of the emitting sources and inadequate spectral resolution to define accurately the physical conditions within the regions. Somewhat later, observations of solar flares with improved spatial resolution but still with broad-band spectral sensitivity (approximately 2-14 Å) demonstrated that the sources of X-ray emission appeared as long, filamentary structures about 1 arc min long and 20 arc sec in diameter (Vaiana, Reidy, Zehnpfennig, VanSpeybroeck and Giacconi, 1969; Beigman, Grimeva, Mandel'stam,

Vainstein, and Zhitnik, 1969). Vaiana and Giacconi pointed out that, although there were considerable similarities between the shape of the Hα flare and the X-ray distribution, there was in addition a bridge of X-ray emission between the two Hα emission centers on opposite sides of the magnetic neutral line. In 1969, direct flare observations were made in EUV wavelengths (Tousey, 1971) and in hard X-ray wavelengths (Takakura, Ohki, Shibuya, Fujii, Matsuoka, Miyamoto, Nishimura, Oda, Ogawara, and Ota, 1971), but no events had yet been observed simultaneously in two or more spectral regions. Furthermore, all of these observations were of short duration so that the evolution of the flare could not be studied.

With the Goddard Space Flight Center experiment on the OSO-7 satellite, we have had the benefit of prolonged observations so that we have been able to view a number of flares from beginning to end. In addition, we can observe events simultaneously in four wavelengths selected from within the wavelength region 1.8 to 400 Å, and by means of automatic switching can observe up to twelve wavelengths in any six minute period. We thereby collect information on emitting regions in a single event with electron temperatures ranging from 0.05×10^6 K to 30×10^6 K. We will first present such observations made during an Importance 1B flare on August 2, 1972, and then discuss the implications of these data on current flare models.

2. Instrumentation

The Goddard experiment on OSO-7 consists of two X-ray spectroheliographs, covering the wavelength ranges of 1.74 to 7.95 Å and 7.95 to 15.90 Å, and one EUV spectroheliograph covering the range 120 to 400 Å, all of which are co-aligned to within 5 arc sec. The wavelength selection of each instrument is independently controlled by ground command. The spatial resolution of the X-ray instruments is produced by multi-grid collimators with fields of view of approximately 20 by 20 arc sec FWHM, and with less than 5% response at 30 arc sec off axis. The X-ray spectral bands are defined by several balanced filter pairs (Ross, 1926). These filters are made of materials adjacent in the periodic table, and each pair is balanced by adjusting the thicknesses so that their transmissions at a given wavelength are identical except between the K (or L) absorption edges of the two materials. One-half of the collimated radiation for either X-ray instrument is passed through one filter and the other half through the second filter, each beam being measured independently by a proportional counter. The difference between detector outputs so obtained is thus a measure of the incident energy in a well-defined band of wavelengths. This procedure is the same for both X-ray instruments, which differ only in the filter materials and proportional counters used.

The spatial resolution of the EUV spectroheliograph is provided by a Wolter Type II grazing-incidence telescope (Wolter, 1952), which focuses the incident radiation onto the entrance aperture of the spectrometer. The size of the aperture is fixed in one dimension to

a projected angular size of 20 arc sec, but in the other dimension it can be selected to be 10, 20, 40, or 60 arc sec. After passing through the entrance aperture, the radiation strikes a grating at a glancing angle of $7^{\circ}.5$ and is dispersed to a set of Bendix Magnetic Electron Multipliers behind the focal curve of the grating. The spectral resolution of the system is approximately 1Å as determined by the width of the exit slits mounted along the Rowland circle of the spectrometer directly in front of the detectors. There are six exit slits in all, two for each detector. A mask in front of the slit assembly insures that only one of each pair is unblocked at a time, however.

The observations reported here were made while the spacecraft rastered the instrumental viewing directions over a 5 x 5 arc min area of the sun. At the end of each raster, a pulse was generated which stepped the X-ray filter pairs to the next set [see Table 1 for the pass bands of the filter pairs], and which switched the EUV mask so that the alternate set of exit slits was uncovered. Unfortunately, because of telemetry limitations, only two of the three EUV detectors could be monitored. The spectrometer was set so that we recorded raster maps at 246.3Å and 294.9Å, alternating with maps made at 219.0Å and 265.0Å, all with an entrance aperture of 20 x 20 arc sec.

Since a 5 x 5 arc min raster takes 61.44 sec to complete, each EUV line pair was observed every two minutes, approximately. However, there are six sets of filters in each of the two X-ray instruments, so their cycle time was approximately six minutes. (The cycle time is reduced

to three minutes for the bands from 1.74 to 1.90Å and from 14.50 to 15.90Å since filter pairs 1 and 4 in each instrument are identical.)

In addition to having X-ray and EUV detectors, the Goddard experiment contains a small Ebert-Fastie spectrometer with a spectral resolution of about 1Å FWHM for isolating the Hα line of neutral hydrogen. It is fed by the zero order reflection from the EUV grating and therefore measures the Hα radiation from the same location on the solar disk. Comparisons with ground-based observations then allow us to determine accurately the spatial scale and orientation of our spacecraft data.

The final component of the Goddard OSO-7 experiment is an X-ray polarimeter which is based on the principle of incoherent Thomson scattering in a beryllium block. The central scattering block is surrounded by six proportional counters, wired together into three pairs, whose relative count-rates indicate the degree of polarization of the incident X-rays. The polarimeter nominally measures X-rays in the energy range of roughly 13 to 30 keV, although the actual range will vary somewhat depending on the spectrum of the incident beam.

3. Data Selection

In order to evaluate the extent to which the EUV data may be contaminated by the appearance of unidentified flare-associated emission lines or enhanced background at the specified wavelengths, we have examined spectra of a large flare on August 7, obtained after flare maximum. The emission line at 246.3Å is found to be significantly weakened relative to the background (being five times more intense than the background in active region spectra but only one-half the intensity of the background during the flare). On this basis the spectroheliograms obtained at this setting are considered to be unreliable. The 265.0Å channel is sufficiently close to the Fe XIV transition at 264.80Å (Behring, Cohen and Feldman, 1972) to monitor the intensity of this line in active regions, but it seems to be blended with other lines in the flare spectrum, and so is also unreliable for the present study.

Of the two remaining spectral positions, that at 294.9Å corresponds to no known or observed spectral line either from the quiet sun, active regions or flares. The signal recorded at this position is therefore presumably due only to scattered radiation in the spectrometer, which always appears to be about 0.15% of the intensity of the nearby, very strong 303.8Å line of He II. Scattered light may also arise from H I emission, since it contributes nearly 90% of the solar photon flux below 1300Å (Hall and Hinteregger, 1970), the wavelength range to which our lithium-fluoride coated photocathode is sensitive. In any case, we assume that the signal at 294.9Å is a rough measure of emission originating in the solar chromosphere.

The remaining EUV wavelength at 219.0 Å monitors the $3s^2 3p\ ^2P_{3/2}$ - $3s^2 3d\ ^2D_{5/2}$ transition of Fe XIV. In the flare spectrum the emission line at this wavelength has a peak intensity three times greater than the level of the underlying continuum, part of which may be continuum due to recombination onto He III, although much of it is radiation scattered by the grating. It is of interest to note that the calculations of Blaha (1971) predict that the transition at 219.0 Å should become stronger relative to $3s^2 3p\ ^2P_{3/2}$ - $3s^2 3d\ ^2D_{3/2}$ at 220.07 Å as the electron density increases from 10^8 cm^{-3} to 10^{11} cm^{-3}. Our comparison of active region spectra with flare spectra confirms this prediction.

As a result of the above discussion we consider the interpretation of only two of the four EUV wavelengths as being reliable during flares - the 294.9 Å position giving spatial information on emission (principally from H I and He II) formed in the upper chromosphere, and 219.0 Å giving the intensity of a density-sensitive Fe XIV line.

Besides the information from these two EUV wavelengths, we utilized almost all of the available X-ray data from our experiment in the study reported here. Although the analysis to establish the presence of X-ray polarization has not yet been completed, the average output of the polarimeter's three channels was used to give the time profile of the flare's total flux between 13 and 30 keV. Solar radiation is almost entirely bremsstrahlung continuum at these energies, but line emission begins to become important at the lower energies measured by the balanced filter technique with our two X-ray spectroheliographs. Even though their spectral resolution is not truly monochromatic, each Ross filter pair isolates a small enough wavelength band so that usually only one

or two strong emission lines dominate the detector's response, as can be seen in Figure 1 which illustrates the situation for the Long X-ray instrument. The ions that produce the dominant emission measured by each filter pair have already been listed in Table 1.

Taking both the line and continuum emission into account, we have calculated the incident energy in the spectral bands of several of the OSO-7 filter pairs as a function of T_e, based on the work of Mewe (1972). The resultant curves for a constant emission measure of 10^{50} cm^{-3} are shown in Figure 2. Although the emission measure actually drops rapidly with increasing T_e in any realistic flare model, each curve clearly indicates the temperature range in which the filter pair is most sensitive.

The only X-ray data not directly used in this study were produced whenever all filters were removed from the optical path of the spectroheliograph. In such cases, the difference in the count rates from the two halves of the system provided a test of its balance.

4. Observations

The selected OSO data taken during the event will be considered in two ways. First, we will examine the intensity of the flare emission as a function of time without regard to the location of that emission. Second, we will consider the spatial distribution of the flare radiation. Because this particular flare developed so rapidly only the EUV data, with a cycle time of 2 minutes, could be used to determine the progress of intensity with time. The EUV intensities, given in units of counts per 0.125 sec at the point of greatest intensity, are plotted as a function of time in Figure 3. A plot of the total flux at each wavelength (obtained by summing all enhanced intensities over the flare's area) would be similar except that the flux remains relatively higher after 1842 UT. The characteristics we observed are:

1. A low preflare intensity at the position where the flare ultimately appears and no detectable preflare enhancement up to 1837:37 UT.
2. An initial rapid brightening, already in progress at 1838:57 UT, which reaches a maximum within one minute of 1840 UT in the Fe XIV emission and perhaps also in the chromospheric emission. This maximum is coincident with an impulsive microwave burst reported by the Algonquin Radio Observatory of the National Research Council of Canada in the Solar-Geophysical Data Bulletin of the Environmental Data Service of NOAA.

3. A secondary maximum at 1842 - 1846 UT, again in both EUV wavelengths, with an enhancement persisting to the end of the observing sequence at 1853 UT.

The soft X-ray observations, because of the longer time between repeated observations in the same wavelength band, are not useable for establishing the variation of soft X-ray emission with time. However, the intensity in the band from 1.74 Å to 1.9 Å have been compared to the estimated continuum flux at 6.7 keV as a function of time as derived from an extrapolation of data supplied by D. Datlowe from the University of California at San Diego (UCSD) hard X-ray instrument on OSO-7. From this comparison it appears that our data are consistent with a rapid rise in soft X-ray flux from 1839 to 1840 UT, with a broad maximum lasting from 1840 to 1844 UT. By comparison, an impulsive X-ray burst, observed both by the UCSD instrument at photon energies from 44 to 216 keV and by the Goddard X-ray polarimeter at 13 to 30 keV, was observed to have a sharp maximum at 1839:40 UT, concurrent with the probable maximum in the EUV emission. These data are consistent with earlier observations of events at EUV wavelengths (Hall and Hinteregger, 1969; Donnelly, 1969; Neupert, 1969). It has been found that such impulsive events are associated with emission lines such as O V produced in the transition region (Hall and Hinteregger, 1969; Hall, 1971; Kane and Donnelly, 1971; Wood, Noyes and Reeves, 1972), or with radiation formed in the high chromosphere, such as the Lyman continuum (Wood, Noyes and Reeves, 1972). Coronal emission lines from high stages of ionization of iron, such as Fe XV and Fe XVI, do not in general

exhibit an impulsive component but become prominent later in the event, either concurrently with the soft X-ray peak or even later (Hall and Hinteregger, 1969; Neupert, White, Gates, Swartz and Young, 1969). In the present event, we observe that the rapid enhancement associated with the chromospheric emission at 294.9Å extends to the Fe XIV ion formed at $T_e \approx 2 \times 10^6$ K. However, the Fe XIV emission remains high after 1843 UT while the chromospheric radiation diminishes.

Table 2 presents data on the enhanced flux at three of the wavelengths that were observed. Interpolations in the 294.9Å data were based on the assumption that 294.9Å intensities varied by the same fractional amount as the 219.0Å intensities during the impulsive phase. Interpolations in the 1.74 - 1.90Å band were obtained by fitting intensities derived from the UCSD data, extrapolated to 1.87Å, to our observed values. Data in the 13-30 keV band were derived from the average output of the three channels in our X-ray polarimeter. We observe the typical pattern of maximum chromospheric enhancement occurring during the impulsive phase and coinciding with the hard X-ray and microwave peaks. It is noteworthy that at 1838:38 UT the chromospheric brightening was already at 18% of its maximum value whereas the hard X-ray emission between 13 and 30 keV has only attained 2% of its ultimate intensity.

Maximum enhancement in the 1.74 - 1.90Å band, which includes the prominent emission lines of Fe XXV, is reached about one minute after the microwave and hard X-ray peak. Maximum emission in the band containing the Fe XVII lines occurs even later. It has been suggested by Neupert et al. (1969) that the progressively later maxima in lower stages of ionization could

be attributed to successive recombinations in a cooling plasma. Although this explanation still seems to be valid, we will be able, after examining the spatial distribution characteristics, to add significantly more detail to such a model.

Up to this point we have not introduced the spatial information contained in the OSO-7 data and have not been able to comment on the proximity of the emitting regions in space as well as in time. We now will do so, by considering in turn the spatial emission of the preflare radiation, the emission associated with the impulsive phase and that emitted after the impulsive event.

Figure 4 compares the intensity contours obtained prior to and during the impulsive phase of the flare. These spectroheliograms are constructed by sweeping the instrument back and forth over the five arc minute field in sixteen lines spaced 20 arc sec apart. In these and all subsequent displays of the data, the intensity steps between contours are scaled to one-eighth of the maximum intensity recorded in the raster. It is therefore possible to compare spatial distributions taken at various wavelengths and to detect changes in spatial distribution in the presence of fluctuations of intensities. Using this method, we note in Figure 4 that at all wavelengths the flare-associated emission is so large that the lowest level of the flare contours is in general greater than the maximum output recorded anywhere in the field of view prior to the flare. More importantly, the position at which the flare appears does not correspond to the location of maximum preflare emission, either at the EUV wavelengths or in the soft X-ray bands containing the Mg XI or the Fe XVII lines (no emission whatever was recorded in the bands near 1.9Å prior to the flare). Indeed, the only region observed

to be emitting X-rays three minutes prior to the event is associated with one of the three regions observed to be bright in Hα, and is located 1.2 arc min (50,000 km) from the flare site. The data have not been corrected for the smearing produced by the raster motion of the spacecraft or the limited spatial response of the system, but such corrections would only serve to emphasize that the flare does not originate in any prominent coronal structure existing prior to the flare.

Representative observations at XUV wavelengths during the flare are shown in Figures 5, 6 and 7. The EUV observations in Figure 5 are selected to demonstrate the evolution in the spatial distribution of the radiation observed during the event. In Figure 6, we compare soft X-ray data for three selected bands containing the helium-like and hydrogen-like emission lines of Ne, Mg and Si (the first two being obtained with the Long X-ray spectroheliograph, the third being recorded by the Short X-ray spectroheliograph). Finally, in Figure 7, we show a sequence of X-ray rasters which include observations of the Fe XXV emission at 1.86 Å.

During the impulsive phase, which lasts from 1838:30 to approximately 1842 UT, the flare has a very similar appearance in the radiation of He II (observed indirectly in Figure 5 by its radiation scattered off the grating), Fe XIV (also in Figure 5) and the Mg XI band (Figure 6). In each case the source is elongated in a northwest-southeast direction with a well-defined bend north of the position of maximum emission. We estimate that at this time the source has an overall length of 36 arc sec (27,000 km) and a width that is small compared to the spatial response of the observing systems. When we observe near 1.9 Å, however,

the region has a distinctly different location and geometry. This can best be seen in Figure 7. First, we must emphasize that when both Long and Short X-ray spectroheliographs are recording longer wavelength radiation (e.g., at 1840:41 UT when one system is recording the band containing the Mg XI and Mg XII lines while the other is observing the Si XIII and Si XIV lines), the observed spatial distributions are similar. However, when the Short X-ray system observes in passbands near 1.9Å, the spatial distribution is distinctly different, even though the distribution recorded at the same time by the Long X-ray system has not changed. Such an effect has not been observed in flare events occurring near central meridian (this event was located 30° east of the meridian). Neither has any malfunction in the operation of the X-ray spectroheliographs or instability in the alignment of the collimating systems ever been observed. We conclude that this displacement of the source emitting 1.9Å X-rays is real and amounts to approximately 24 arc sec (17,000 km) measured normal to the line of sight. Actually, this separation of emitting sources is not unexpected since no single ion can persist over the large range of electron temperatures (5×10^4 K - 30×10^6K) which are found in this flare, (cf. Section 6).

Let us consider now the evolution of the flare after the impulsive event. Figure 5 shows that after 1842 UT, as the impulsive event was coming to an end, the EUV emission at both wavelengths has moved northward from its original location, and by 1845 UT the points of maximum intensity no longer coincided. The chromospheric source (294.9Å) has elongated and remains north of its original position until 1848 UT. On the other hand, the

Fe XIV source (219.0Å), while somewhat more extended than originally, does not exhibit the degree of elongation observed at 294.9Å. Furthermore, by 1845 UT the maximum intensity of the Fe XIV source has returned to the original position observed at 1839:39 UT. The chromospheric source does not return to its original location until 1848:52 UT.

Examining the spectroheliograms taken in the soft X-ray bands (Figure 6), we find that the source may be elongating somewhat more slowly than was observed at EUV wavelengths. The location of maximum emission remains fixed, at least until 1845 UT. The fact that the passbands of some of the filters include more than one spectral line and continuum emission formed over a wide range of electron temperature (see Figure 2) may account for the similarity in the spatial distribution of the source in several of the soft X-ray spectral bands. There is also some evidence in the data taken after 1851 UT that the center of the emission has moved northward and an indication in the 13.30 - 14.50Å and 7.95 - 9.51Å bands that a double maximum may be evolving.

Considering finally the spectroheliograms in the emission lines and continuum near 1.9Å which record the spatial distribution of the quasi-thermal plasma having the highest temperature observable with the instrument (Figure 7), we find that the position of the source does not change throughout the entire event. In addition, its size remains always below the resolution limit of the spectroheliograph, indicating that the hot plasma is somehow contained, possibly within a stable magnetic configuration. This is consistent with the trend toward a greater compactness with increasing electron temperature already observed in the emission lines formed at lower temperature.

5. Comparison with the Associated Hα Flare

The X-ray and EUV spectroheliograms can be compared with ground-based filtergrams using data from the auxiliary Hα system contained within the instrument. The satellite-borne Hα monitor has the same spatial resolution as does the EUV (approximately 20 arc sec), and a FWHM passband of about 1Å. Although these figures are poor relative to ground-based equipment, the spectroheliograms so obtained show adequate differences in signal from bright plage and from sunspots to establish the spatial relationship between satellite and ground-based observations. Because of telemetry restrictions, the OSO-7 Hα data could not be taken simultaneously with the XUV data. Observations were taken three hours after the flare, however, and corrected for solar rotation to properly register our XUV data with off-band Hα photographs made at the Lockheed Solar Observatory and kindly supplied to us by S. Martin.

The results of these comparisons are given in Figures 8 through 11. The spatial distribution of the XUV radiation during the impulsive phase of the event is shown in Figure 8. In all emission lines produced at 10×10^6 K or less, the XUV source coincides with the off-band Hα distribution to within the accuracy of the spatial comparison, i.e., about 5 arc sec. Figure 8a shows this relationship using the EUV data at 294.9Å. However, even during the impulsive hard X-ray burst, the source of radiation at 1.9Å has a different shape, with its most intense point lying to the north and east of the Hα emission. It should be noted

that the 1.9Å spectroheliogram scanned through the vicinity of the flare within 10 sec of the maximum amplitude of the impulsive hard X-ray emission.

As the event progresses, the Hα emission elongates toward the north, and a break appears in the bright Hα filament as it curves around a sunspot. A comparison with magnetograms taken after the event by W. Livingston of Kitt Peak National Observatory indicates that the break in the bright filament occurs in a region of high magnetic field gradients and very near the neutral line. We suggest that the northern and southern positions of the Hα filament may therefore be lying on opposite sides of the neutral line.

Figures 9 and 10 provide a comparison of XUV emission with Hα after the impulsive phase. The chromospheric radiation (294.9Å) still corresponds well to the Hα emission, although it may also be associated with a dark, northward-moving surge observed in Hα. The Fe XIV emission maximum, on the other hand, is again centered at its original location (after having moved to the north at 1841 UT). An elongation to the north does remain and coincides precisely with the northward moving surge. The sources of emission at 5.02-7.95Å and 7.95-9.51Å show less extension to the north with time. The maxima at these wavelengths coincide with the break in the bright Hα filament. The spectroheliograms at 1.9Å show that no motion whatever has occurred in this source from 1839 to 1846 UT; it remains located to the north and east of the other emissions and is observed against a background of low magnetic field gradients. Note that the emission appears at the point where the dark surge becomes visible.

To summarize these results:

1. No coronal feature is recorded at the site of the flare prior to the event.

2. During the impulsive phase, all emissions except at the shortest observed wavelength (1.9Å) have similar spatial distributions and match the most intense region of Hα emission observed off-band at 1839 UT. The maximum emission occurs near a region of high gradients in the longitudinal magnetic field and, in fact, extendsbetween regions of opposite polarity, crossing the neutral line at an oblique angle.

3. During the post-impulsive phase of the event, the best correlation with the structure of the off-band Hα flare brightening is found in emission assumed to originate in the high chromosphere. Correlation with a dark surge appears to be best in the emission of Fe XIV. Emission originating at higher electron temperatures exhibits a tendency to remain more compact and stationary. For emission characteristic of 2.5×10^6 K $< T_e < 10 \times 10^6$ K, the most intense region of the XUV flare is over a break in the bright Hα filament which may represent the boundary between magnetic fields of opposite polarity.

4. The radiation at 1.9Å appears to be displaced relative to the other emitting regions. Moreover, it seems to remain fixed in position and perhaps in size, at least during the first 8 minutes of the event when its intensity is adequate for reliable observations.

6. Physical Properties of the XUV Flare

Since the spatial resolution of the instrument is limited at all wavelengths and the spectral resolution in the X-ray region is inadequate to isolate individual spectral lines, the calculations of physical parameters can at best be only estimates. We will consider three spectral regions: (1) The wavelength of 219.0Å at which the $3s^2 3p\ ^2P_{3/2} - 3s^2 3d\ ^2D_{5/2}$ transition of Fe XIV is emitted; (2) the spectral band from 7.95 to 9.51Å including the resonance transitions of Mg XI and Mg XII; and (3) the spectral band from 1.74 to 1.90Å including the transitions of Fe XXV. The relative strengths of line emission and continuum in the X-ray bands can be estimated from spectra taken by OSO-5 on February 27, 1969, during a flare of importance 2b. From Neupert, Kastner, and Swartz (1973) we find that during this event the Mg XI transitions represented 18% of the total emission in the 7.95 - 9.51Å spectral band. For the same event the ratio of Mg XII to Mg XI line fluxes corresponded to $T_e = 9.4 \times 10^6$ K, based on the calculations of Mewe (1972). We will adopt this temperature in our analysis. From Saba (1972) and Neupert and Swartz (1970) we find that the Fe XXV transitions account for 37% of the total radiation in the band between 1.74 and 1.90Å. For this region we assume $T_e = 30 \times 10^6$ K, compatible with the analysis of Saba (1972). Finally, at 219.0Å, 75% of the count rate is due to Fe XIV emission, the remainder being undispersed radiation scattered by the grating. For this ion we assume $T_e = 2.3 \times 10^6$ K, the temperature at which the relative population of Fe XIV is a maximum (Jordan, 1969).

The fluxes in these three spectral regions are given in Table 3 for the time near 1842 UT, just after the impulsive phase of the flare on August 2, 1972. The emission measures listed for Fe XXV and Mg XI are based on the calculations of Mewe (1972), which assume that the excited levels are populated only by collisional excitation from the ground state. Average electron densities can then be derived if the volume of the emitting region is known. In this case the volumes given in Table 3 represent only upper limits. Based on our previous discussion, the sources are assumed to be loop-like structures whose length is taken to be the distance between half-intensity levels, measured along the long dimension of the source. Because of uncertain projection effects, this length may be in error by as much as a factor of 2. The observed width of each source is equal to that expected when the dimension is small compared to the resolution of the collimators. In the absence of a reliable value, we will adopt 5 arc sec as the width of the loops in these three cases. The volume we find for the X-ray and EUV emitting plasma is then no greater than 6.7×10^{26} cm^3 for any of the three emitting regions. [It is of interest to note that Vaiana and Giacconi (1969) estimated a volume of 1.2×10^{27} cm^3 (equivalent to a 15 arc sec cube) for the X-ray emitting plasma of a flare of importance 1.] Estimates of the electron density and total kinetic energy in the gas are also given in Table 3.

Blaha (1971) has shown that the excited levels of Fe XIV are populated by cascades from upper levels as well as by collisional excitation from the ground state. For the Fe XIV radiation, therefore, the flux at the earth is given by

$$F = \frac{1}{4\pi R^2} \int n_{ion,2}\, A_{21}\, h\nu dV,$$

where $n_{ion,2}$ is the population of the excited $3s^2 3d\ ^2D_{5/2}$ level and A_{21} is the Einstein rate coefficient to the ground state. This expression is equivalent to

$$F(\text{erg cm}^{-2}\ \text{sec}^{-1}) = \frac{7 \times 10^{-36}}{\lambda(\text{Å})} \int \frac{n_{ion,2}}{n_{ion}} \frac{n_{ion}}{n_{element}} \frac{n_{element}}{n_{hydrogen}} \frac{n_{hydrogen}}{N_e} N_e\, A_{21}\, dV.$$

The fractional population in the excited state $n_{ion,2}/n_{ion}$ is tabulated by Blaha (1971) as a function of electron density;

$\frac{n_{ion}}{n_{element}}$ is given by Jordan (1969) and we adopt its maximum value for Fe XIV (i.e., 0.210) which is reached at $T_e = 2.3 \times 10^6$ K; the elemental abundance of iron relative to hydrogen $\frac{n_{element}}{n_{hydrogen}}$ we take as 1×10^{-4} (deBoer, Olthof and Pottasch, 1972); and finally, $\frac{n_{hydrogen}}{N_e}$ we take as 0.8 in the corona; the gf-value is given by Blaha (1971) as 2.46 for this transition, which means $A_{21} = 5.7 \times 10^{10}\ \text{sec}^{-1}$.

The mean electron density is obtained, for a given volume (again as an upper limit), by finding that value of $n_{ion,2}/n_{ion}$ (and hence electron density) which yields a calculated N_e consistent with the initially assumed N_e. The emission measure listed in Table 3 for Fe XIV follows from this derived density.

Because of the sequence in which the data were taken, the observations used for Table 3 were not simultaneous, but were separated by one minute in time. We believe, however, that the figures represent reasonable estimates of the physical conditions within the quasi-thermal plasma near the end to the impulsive phase of the flare. It is true that the flux at 1.9Å appears to have remained nearly constant from 1840 to 1844 UT, based on our extrapolation of X-ray observations obtained by the UCSD hard X-ray monitor on OSO-7, and therefore one could argue that the non-thermal impulsive phase is still in progress at 1842 UT, the time of our analysis. On the other hand, if we estimate the e-folding collision loss-time for fast electrons interacting with an ambient material of density n_o as

$$\tau_{coll}\ (E_e) \approx \frac{10^8}{n_o}\ E_e\ (\text{keV})^{3/2}\ \text{sec}$$

(Trubnikov, 1965; Kane and Anderson, 1970), we find, for E_e = 100 keV and $n_o = 1 \times 10^{11}\ \text{cm}^{-3}$,

$$\tau_{coll} = 1\ \text{sec.}$$

Therefore, thermalization proceeds rapidly compared to the 2-3 minute duration of the impulsive burst (implying, however, that there must be a continuous injection of electrons during this time). This suggests that the assumption of a quasi-thermal plasma may be reasonable in our analysis, even in the case of the 1.9Å radiation.

We can now consider the question of the origin of the X-ray emitting plasma. We estimate from Figure 3 that a preflare coronal enhancement in Fe XIV at the site of the flare could not have been greater than

5% of the maximum flare emission. This would have corresponded to an emission measure of 1.6×10^{46} at a nominal coronal temperature of 2.3×10^{6} K. The fact that during the flare emission measures greater than this were observed at all temperatures up to 30×10^{6} K demonstrates that the flare emission could not be due simply to the heating of such a pre-existing coronal structure. The possibility that a form of pinch effect is responsible for a compression of the material, thus increasing its emission measure, appears to be ruled out by the fact that this would require a collapse of the emitting region's volume by a factor of 100, which is not observed. We conclude therefore that the plasma originated as a result of heating and ionization of material originally at near-chromospheric temperatures. Additional confirmation of this explanation is found in Table 2 where we note that the initial enhancement appears to occur most rapidly in emission lines formed at chromospheric temperatures.

7. Discussion of the Observations

We have, up to this time, not discussed the possible spatial relationships between the several soft X-ray emissions. The fact that the 1.9Å X-ray emission does not coincide with any well defined photospheric magnetic feature whereas the longer wavelength radiations do, suggests to us that the shortest wavelengths originate at a greater height above the photosphere. More specifically, we hypothesize that the 1.9Å radiation may be emitted from an arch-like structure which is highest directly above the break in the bright Hα filament, its height at this point being about 35,000 km, based on the apparent eastward displacement of the X-ray source and the 30° E longitude of the flare. The arch would have its footpoints in or above the portions of bright Hα filaments nearest to the break but have little or no physical connection with the extremities of the Hα flare.

To fit such a picture to the remaining data, we suggest a model of the arch structure in which there is a nearly potential magnetic field at lower altitudes with lines of force having their planes almost normal to the neutral line between the sunspots that are labeled f_1 and p_3 by Zirin and Tanaka (1972). At higher altitudes the field lines become severely sheared with footpoints near these two sunspots. The high temperature source emitting at 1.9Å is at the level of the strongly sheared field, while the radiation of the cooler Fe, Mg, and Si sources is formed at the level of the potential field. It should be pointed out that Tanaka and Nakagawa (1973) have proposed a model for the great flare of August 7, 1972, in this same active region, that also implies that the magnetic field becomes increasingly sheared with height.

Our observations do not permit us to say anything about the spatial configuration of material at intermediate temperatures, and therefore presumably intermediate heights. On the other hand, we believe that there must be a connection between the two sets of field lines to allow for the rapid transfer of energy between them. There might be, for instance, a current sheet configuration at intermediate heights similar to that considered by Sweet (1958), who argues that magnetic field reconnection takes place in this region, thus providing the source of the flare's energy. Such a configuration would satisfy the requirements of both the XUV and Hα observations insofar as it provides a means of quickly dumping energy at chromospheric levels to produce short-lived Hα kernels and also a source of energetic electrons trapped at coronal heights which ultimately heat the evaporated chromospheric material to temperatures as high as 30×10^6 K.

To account for the mass motion observed at $T_e < 2 \times 10^6$ we must assume that only a fraction of the material which is evaporated from the vicinity of the chromosphere or transition region during the initial stages of the flare is trapped along the closed magnetic field lines described above. The remainder is either injected with adequate kinetic energy to escape from the closed field region or injected into a region of open field lines, in either case contributing to the observed surge. Such a possibility has already been discussed by Gold (1968).

Using this model, we are now able to discuss the further evolution of the flare plasma after the impulsive phase. We recall that the source of 1.9Å emission fades rapidly after 1846 UT, so that we have no reliable observations of it after that time. We observe in Figure 6, however, that by 1852:59 UT the peak of the 5.02-7.95Å emission occupies the site originally emitting at 1.9Å. Moreover, the emission between 7.95 and 9.51Å has elongated so that it includes not only the original site of that emission but also the region originally emitting at 1.9Å. On the other hand, observations in the band containing the Ne IX lines show that its source remains fixed in space. We propose that these data give direct evidence of the cooling of the emitting plasma after the impulsive phase. Referring again to Figure 2 which gives the emission in the bands of seven of our Ross filter pairs as a function of T_e for an emission measure of 10^{50} cm^{-3}, we argue that originally just the hottest (and highest) arch system can have had a T_e such that it radiated strongly only at 1.9Å, i.e., it must have had $T_e = 30 \times 10^6$ K. The lower arch system, which was observed to have nearly the identical geometry in all three spectral bands above 5Å, must have had regions with 2×10^6 K $\leq T_e \leq 20 \times 10^6$ K.

By 1852 UT, the upper arch system was emitting not at 1.9Å, but in the 5.02 - 7.95Å band. It must therefore have cooled so that $T_e \leq 20 \times 10^6$ K. On the other hand, this feature was not emitting in the Ne IX band, so that it must have had $T_e > 10 \times 10^6$ K. The upper arch had therefore cooled from 30×10^6 to $10\text{-}20 \times 10^6$ K in 12 minutes. Also, by 1852 UT the lower arch system was no longer

a strong emitter at 5.02 - 7.95Å. Its maximum temperature could therefore be no greater than 5×10^6 K after that time. Thus, the apparent changes in source location are nothing more than the result of changing T_e with time. The arch systems themselves have remained essentially fixed in space while the maximum T_e has dropped by a factor of ~2 and the temperature gradient with height above the neutral line has lessened.

These conclusions clearly demonstrate the intrinsic limitations of spectral observations made without spatial resolution. The "average" properties of the flare that are deduced from such data may have little resemblance to the actual physical characteristics of the flare. In instances where we observe the enhancement and decay in particular spectral lines or bands, for example, the emission from one region of the flare may be increasing while, at the same time the emission from another region is diminishing.

A feature our picture has in common with previously discussed models (deJager and Kundu, 1963; Takakura and Kai, 1966; Sturrock, 1968; Strauss and Papagiannis, 1971) is the presence of a magnetic flux tube or loop originating in a magnetic field region of one polarity and connecting to a region of opposite polarity. In this flux tube are found energetic particle streams (accelerated in Sturrock's model as the result of reconnection of magnetic field at the neutral sheet formed by open field lines above the closed field configuration). Another property of these models is that the energetic particles,

arriving at the footpoint of the flux tube, produce a hot X-ray emitting plasma and may also be responsible for the bright Hα points observed simultaneously with the impulsive hard X-ray burst (Vorpahl and Zirin, 1970). Although we do indeed observe at least one loop system and perhaps several, the region of maximum emission (especially for 2.5×10^6 K $< T_e < 10 \times 10^6$ K) is greatest not on either side of the neutral line, i.e., above the bright Hα filaments seen later in the flare, but directly above the break between those filaments where we suppose the neutral line to be. The data are therefore difficult to reconcile with the production of Hα emission by the penetration of fast particles into the chromosphere as had been suggested by Vorpahl and Zirin (1970). A similar conclusion has already been made by Takakura (1971) on the basis of hard X-ray observations of a flare made by Takakura and co-workers (1971). An alternative possibility, of course, is simply that our instrument has inadequate spatial resolution to establish the relationship between soft X-ray and Hα emission.

One fact which the data clearly establish, however, is that the highest electron temperature is not found (even during the impulsive phase) immediately above the chromosphere, where the fast electrons are presumed to be heating the material. The location of the 1.9Å source requires that the electron temperature increase from about $5\text{-}10 \times 10^6$ K directly above the chromosphere to 30×10^6 K at a height of 35,000 km. Thus, heating and ionization must occur over this range of heights. Such a requirement does not, however, rule

out the possibility that non-thermal bremsstrahlung is produced as the result of deceleration of electrons in the chromosphere. A dynamic model of the event would have to account for an initial heating of material, perhaps produced by collisional losses of high energy electrons in the chromosphere (Neupert, 1968), followed by additional heating at heights of 10,000 km or more above the chromosphere. Such heating could be produced by high energy particles trapped in a closed magnetic field configuration which as yet have not impacted on the chromosphere or escaped into the high corona. The entire range of heights over which this heating must occur is not observable at any single wavelength since it encompasses a wide range of electron temperatures. From an inspection of our present data we conclude, however, that at 1839 UT it extends from the 294.9Å source observed in the high chromosphere (Figure 5) to the source observed at 1.9Å at which the highest electron temperature is to be found (Figure 7).

Strauss and Pagagiannis (1971) have used the model of Sturrock and Smith (1968) and Sturrock (1968) to calculate the expected densities and temperatures in a loop when the injection of energetic particles occurs at the top of the loop. Using an injection rate which is chosen to give consistent results at the beginning of the event, they are able to match the observations for the post-maximum phase of an X-ray burst recorded by OSO-5. They are best able to fit the data with a loop height of 57,000 km, maximum T_e of 61.7×10^6 K, and $N_e = 4 \times 10^{11}$ cm^{-3}. These conclusions are based on a cross-sectional loop area of 7.5×10^{14} cm^2. If this were to be increased

to the dimension we have used (9×10^{16} cm^2) and the loop height decreased by a factor 2, we estimate that the calculated electron density would be only a factor of 3 higher than what we have reported earlier in this paper. However, a difficulty remains in that we find no supporting evidence for the hypothesis that energetic particles are injected at the top of our loop and thermalized at the footpoints. A similar analysis has recently been carried out by Sturrock (1972). His results for a small intense flare having a hot plasma loop 30,000 km long are also in general agreement with our observations.

Culhane, Vesecky and Phillips (1970) have considered the cooling mechanisms for loops such as we have observed. Although they were able to rule out collisions of electrons with lower temperature ions as the cooling mechanism, they were not able to discriminate between cooling by conduction and by radiation on the basis of available data. In our case, however, the fact that the loop at 1.9Å is observed for more than 6 minutes (i.e., $T_e > 10 \times 10^6$ K for this duration) places constraints on any possible model. Since the radiation cooling rate per unit emission measure is nearly constant at a value of 10^{-23} erg sec^{-1} for temperatures between 10×10^6 and 30×10^6 K, we may write

$$\frac{dE}{dt} = 3\, N_e V\, k \frac{dT}{dt} = 10^{-23}\, N_e^2\, V \text{ erg sec}^{-1}$$

or

$$\Delta t = \frac{3k\ \Delta T}{10^{-23}\ N_e} \text{ sec.}$$

Using $\Delta T = 20 \times 10^6$ K and $N_e = 1.5 \times 10^{10}$ cm^{-3}, we find $\Delta t = 5 \times 10^4$ sec, which is more than a factor of 100 longer than the observed duration. N_e would therefore have to be greater than 2×10^{12} cm^{-3} if the rate of cooling were due only to radiation. As this density is unrealistically high, we feel that radiation cooling is not important in the present instance.

Consider now the possibility of conduction cooling. Culhane et al. (1970) discuss conduction models for several values of a parameter α, where $\alpha \approx 2 \times 10^{10} N_e^{-1} \ell^{-2}$, and ℓ is the length of the arch in cm. Using $\ell \approx 6.4 \times 10^9$ cm and $N_e = 1.5 \times 10^{10}$ cm^{-3}, we find $\alpha = 3.2 \times 10^{-20}$. For this value of α the graphs presented by Culhane et al. (1970) show that conduction would cause T_e to drop to 10×10^6K in 90 sec, i.e., more rapidly than observed. An increase in N_e would only produce a greater discrepancy. We therefore conclude that the hot plasma may not be coupled directly to the chromosphere but may rather be contained in a partially leaky magnetic bottle which permits a conduction cooling rate about 4 times less than otherwise would be the case. Under such circumstances we expect that radiation cooling could still have a minor role.

In addition to the direct observations of loop-like or filamentary structures emitting soft X-rays (Vaiana et al., 1968; Beigman et al., 1969), indirect evidence for an arch-like structure emitting soft X-rays as well as Hα radiation has been presented by Zirin, Ingham, Hudson and McKenzie (1969). Their argument is based on the observation that the flux measured in the 7.7 - 12.6 keV

spectral region by the UCSD instrument on OSO-3 is well correlated with the projected area of a rising Hα arch during the increasing phase of an X-ray burst. Although Zirin et al. reported a maximum height of 46,000 km for their arch, a figure comparable to our results, there exist significant differences which make it unlikely that our loop at 1.9 Å can be attributed to the same type of feature observed by them. In the first place, their Hα feature rose at a nearly constant velocity (we estimate a component normal to the line of sight of 136 km sec^{-1}). The feature we report remains fixed throughout the observing interval although motion would easily have been detected. Secondly, Zirin et al. concluded that the radiating electrons were uniformly distributed throughout the arch (because of the smooth rise with time in the X-ray flux). Our feature is definitely not uniform in intensity - one side is obviously more intense than the other. If it were to rise from behind the limb at the rate observed by Zirin et al., it would reach nearly maximum visibility in soft X-ray emission in about 25 sec. Such a sharp increase was not observed in the OSO-3 data.

Efforts to define the region in which electron acceleration takes place have as yet produced no conclusive results. Zirin, Pruss and Vorpahl (1971) argue, from the apparent frequency cutoff in radio emission during one event, that the process must take place at densities of 10^{11} cm^{-3} or at an initial temperature of 30,000 K. Kane and Lin (1972) on the other hand argue, from the detection of low energy interplanetary electrons, that the acceleration occurs at

$10^9 \leq n_i \leq 10^{11}$ cm^{-3}. We are not able to identify any coronal structures prior to the flare that might provide the site for electron acceleration. A possible solution to the dilemma may be in our observations that some field regions are closed and effectively trap the high temperature plasma while others are sufficiently open to permit the ejection of material. Thus, it might be possible for energetic electrons to "leak" around an overlying cloud of high density plasma which provides adequate attenuation for the line of sight radio emission.

8. Summary

On the basis of spectroheliograms at selected wavelengths throughout the XUV region, we come to the following conclusions.

1. There is no detectable coronal feature at the site of the flare prior to the event. Heating only the pre-existing coronal material cannot account for the flare emission.

2. Flare emission at $T_e \leqslant 2.3 \times 10^6$ K exhibits an impulsive component which has already reached 18% of its ultimate intensity at 1838:38 UT when X-rays at wavelengths below 2 Å are just beginning to be emitted. This suggests that the flare has its origin in the chromosphere or transition region and that energy losses by high-energy electrons may not be necessary for the production of the impulsive chromospheric radiation.

3. With the exception of the highest temperature plasma, the source of the radiation associated with the impulsive phase follows the neutral line between fields of opposite magnetic polarity. The emission is centered at a break in the bright Hα flare filament which probably separates the two magnetic field regions. There is no close correspondence between the spatial distributions of the Hα brightening and soft X-ray emission after the impulsive phase, however.

4. At least two distinct structures are observed at X-ray wavelengths. From the wavelengths at which emission occurs, we infer an initial temperature of $2\text{-}10 \times 10^6$ K for one structure which forms immediately over the Hα flare during the impulsive phase. Simultaneously, an arch with $T_e \approx 30 \times 10^6$ K develops about 35,000 km above the Hα event. The regions with highest electron temperature exhibit the

greatest stability in position and perhaps in size. We conclude that the magnetic field lines directly above the principal source of energy dissipation are closed. The observations require that ionization and heating of evaporated chromospheric material continues as the material streams upward. It may therefore be that the region of 1.9Å emission delineates a storage region and perhaps even an acceleration region for high energy electrons. As the particle density increases in this region during the impulsive phase, the collisional energy loss rate will increase and may "quench" the electron acceleration process.

5. From the long lifetime of the high temperature region (at least 6 minutes and perhaps as much as 12 minutes to cool from 30×10^6 to 10×10^6 K), we conclude that this region may be conductively decoupled from the chromosphere. Even so, radiation losses are significantly smaller than conduction losses.

6. In addition to the stationary plasma at high electron temperature, we also observe moving material apparently associated with a dark Hα surge. This is best observed in an emission line of Fe XIV during the post-impulsive phase of the flare. The ejection of this material occurs not from the top of the closed arches but either from below them (and therefore directly at the neutral line) or from the vicinity of the northern footpoints of the arches.

It has become clear to us that the instrument used for these observations is barely adequate to trace the evolution of this complex event. However, even these rudimentary results give ample evidence of the rich fields of observational and theoretical results which remain to be undertaken in the physics of solar flares.

Acknowledgements

Many people have contributed to the success of our program of observations from the OSO-7 satellite. We are greatly indebted for the competent technical management provided to us by Milton Kalet and Gary Harris of the Goddard Space Flight Center and for the contributions of our co-investigator, Dr. James H. Underwood, now at the Aerospace Corporation. Assistance in calibrating and operating the experiment has been provided by Charles Condor, Edward Rothe, Robert McColm, Marvin Swartz and Robert Young. The instrument was built for us by the General Electric Co., Valley Forge, Pennsylvania. We wish particularly to thank Andrew Sterk, Frank Kieser, Earl Knox and Stephen Peck for solving many technical problems and for providing an instrument capable of achieving our scientific objectives. The spacecraft was built by the Ball Brothers Research Corporation and has proven to be a reliable and stable platform for our observations. We wish to recognize the efforts of the OSO Project Office and the OSO Control Center at Goddard in managing the preparation of the spacecraft before launch and providing dependable operations thereafter. Their assistance has been indispensible and is sincerely appreciated. We also wish to acknowledge several informative discussions with Y. Nakagawa on the configurations of magnetic fields in active regions and flares. All Hα photographs in this paper were graciously supplied by S. Martin of Lockheed Solar Observatory. One of us (WMN) would like to express his thanks to Dr. Gordon Newkirk, Director of the High Altitude Observatory, for his hospitality during a sabbatical leave when work on this paper was completed.

References

Behring, W. E., Cohen, L., and Feldman, U.: 1972, Astrophys. J. 175, 493.

Beigman, I. L., Grimeva, Yu. I., Mandel'stam, S. L., Vainstein, L. A., and Zitnik, I. A.: 1969, Solar Phys. 9, 160.

Blaha, M.: 1971, Solar Phys. 17, 99.

Culhane, J. L., Vesecky, J. F., and Phillips, K. J. H.: 1970, Solar Phys. 15, 394.

Datlowe, D. 1972, Private communication.

deBoer, K. S., Olthof, H., and Pottasch, S. R.: 1972, Astron. and Astrophys. 16, 417.

deJager, C. and Kundu, M. R.: 1963, Space Research 3, 836.

Donnelly, R. F.: 1969, J. Geophys. Res. 74, 1873.

Gold, T.: 1968, Mass Motions in Solar Flares and Related Phenomena, J. Wiley and Sons, N. Y., p. 205.

Hall, L. A.: 1971, Solar Phys. 21, 167.

Hall, L. A. and Hinteregger, H. E.: 1969, Solar Flares and Space Research, ed. C. deJager and Z. Svestka, North-Holland Publ. Co., Amsterdam, p. 81.

Hall, L. A. and Hinteregger, H. E.: 1970, J. Geophys. Res. 75, 6959.

Jordan, C.: 1969, Mon. Not. Roy. Astr. Soc., 142, 501.

Kane, S. R., and Anderson, K. A.: 1970,Astrophys. J. 162, 1003.

Kane, S. R. and Donnelly, R. F.: 1971, Astrophys. J. 164, 151.

Kane, S. R. and Lin, R. P.: 1972, Solar Phys. 23, 457.

Livingston, W.: 1972, Private communication.

Martin, S.: 1972, Private communication.

Mewe, R: 1972, Solar Phys. 22, 459.

Neupert, W. M.: 1968, Astrophys. J. 153, L59.

Neupert, W. M.: 1969, Annual Review of Astronomy and Astrophys. 7, 121.

Neupert, W. M., Kastner, S. O., and Swartz, M.: 1973, submitted for publication.

Neupert, W. M., and Swartz, M.: 1970, Astrophys. J. 160, L189.

Neupert, W. M., White, W. A., Gates, W. J., Swartz, M., and Young, R. M.: 1969, Solar Flares and Space Research, ed. C. deJager and Z. Svestka, North-Holland Publ. Co., Amsterdam, p. 95.

Ross, P. A.: 1926, Phys. Rev. 28, 425.

Saba, J.: 1972, Masters Thesis, University of Maryland.

Strauss, F. M., and Papagiannis, M. D.: 1971, Astrophys. J. 164, 369.

Sturrock, P. A.: 1968, Structure and Development of Solar Active Regions, ed. K. O. Kiepenheuer, Reidel Publ. Co., Dordrecht, Holland, p. 471.

Sturrock, P. A.: 1972, Mass Motion in Solar Flares, SUIPR Report No. 498.

Sturrock, P. A., and Smith, S. M.: 1968, Solar Phys. 5, 87.

Sweet, P. A.: 1958, Electromagnetic Phenomena in Cosmical Physics, ed. B. Lehnert, Cambridge University Press, p. 123.

Takakura, T. and Kai, K.: 1966, Publ. Astron. Soc. Japan 18, 5[illegible].

Takakura, T., Ohki, K., Shibuya, N., Fujii, M. Matsuoka, M., Miyamoto, S., Nishimura, J., Oda, M., Ogawara, Y. and Ota, S: 1971, Solar Phys. 16, 454.

Takakura, T.: 1971, Solar Phys. 19, 186.

Tanaka, K. and Nakagawa, Y.: 1973, to be published.

Tousey, R.: 1971, Phil. Trans. Roy. Soc. Lond. A 270, 59.

Trubnikov, B. A.: 1965, Rev. Plasma Phys. 1, 105.

Vaiana, G. S. and Giacconi, R.: 1969, Plasma Instabilities in Astrophysics, ed. D. G. Wentzel and D. A. Tidman, Gordon and Breach, N. Y., p. 91.

Vaiana, G. S., Reidy, W. P., Zehnpfennig, T., Van Speybroeck, L. and Giacconi, R.: 1968, Science 161, 564.

Vorpahl, J. and Zirin, H.: 1970, Solar Phys. 11, 285.

Wolter, H.: 1952, Ann. Phys. (Leipzig) 10, 94.

Wood, Jr., A. T., Noyes, R. W., and Reeves, E. M.: 1972, Solar Activity Observations and Predictions, ed. P. S. McIntosh and M. Dryer, MIT Press, Cambridge, p. 117.

Zhitnik, I. A., Krutov, V. V., Maljavkin, L. P., Mandel'stam, S. L. and Cheremukhin, G. S.: 1967, Space Res. 7, 1263.

Zirin, H., Ingham, W., Hudson, H. and McKenzie, D.: 1969, Solar Phys. 9, 269.

Zirin, H., Pruss, G. and Vorpahl, J.: 1971, Solar Phys. 19, 463.

Zirin, H. and Tanaka, K.: 1973, The Flares of August 1972, Big Bear Solar Observatory Preprint.

Table 1

Short X-Ray Spectroheliograph

Position	Filter Element	λ (Å)	Δλ (Å)	Dominant Emission Lines
1	Fe - Mn	1.74 - 1.90	0.16	Fe XXIV, Fe XXV
2	Mn - Cr	1.90 - 2.07	0.17	Fe satellites
3	S - Al	5.02 - 7.95	2.93	Si XIII, Si XIV
4	Fe - Mn	1.74 - 1.90	0.16	Fe XXIV, Fe XXV
5	Fe - Cr	1.74 - 2.07	0.33	Fe XXIV, Fe XXV
6	(None)	-	-	-

Long X-Ray Spectroheliograph

1	Ni - Co	14.50 - 15.90	1.40	Fe XVII
2	Ge - Zn	10.19 - 12.13	1.94	Fe XVII, Fe XXII, Fe XXIV
3	(None)	-	-	-
4	Ni - Co	14.50 - 15.90	1.40	Fe XVII
5	Cu - Ni	13.30 - 14.50	1.20	Fe XVII; Ne IX
6	Al - Mg	7.95 - 9.51	1.56	Mg XI, Mg XII

Table 2

Time ± 30 sec (UT)	Flux (Total counts per 0.125 sec)				Percent of Maximum Flux			
	294.9 Å	14.50-15.90 Å	1.74-1.90 Å	13-30keV	294.9 Å	14.50-15.90 Å	1.74-1.90 Å	13-30keV
1838:38	994	162	≤12	13	18	6	≤4	2
1839:39	5580 (est.)	1654	285 (est.)	664	100	63	95 (est.)	100
1840:41	4268	2454 (est.)	300 (est.)	385	76	93 (est.)	100	58
1841:42	3067 (est.)	2626	284	206	55 (est.)	100	95	31
1847:50	1728	1850	68	≈0	31	70	23	≈0

Table 3

Characteristics of XUV Flare near 1842 UT

Ion	T_e (10^6 K)	F (erg cm^{-2} sec^{-1})	N_e^2 V (cm^{-3})	V (cm^3)	$\bar{N}_e$ (cm^{-3})	3 $\bar{N}_e$ V kT (erg)
Fe XIV	2.3	1.3×10^{-3}	3.2×10^{47}	$\leq 6.7 \times 10^{26}$	$\geq 2.2 \times 10^{10}$	1.4×10^{28}
Mg XI	9.4	1.4×10^{-4}	3.9×10^{48}	$\leq 3.1 \times 10^{26}$	$\geq 1.1 \times 10^{11}$	1.3×10^{29}
Fe XXV	30	4.8×10^{-6}	7.2×10^{46}	$\leq 3.3 \times 10^{26}$	$\geq 1.5 \times 10^{10}$	6.1×10^{28}

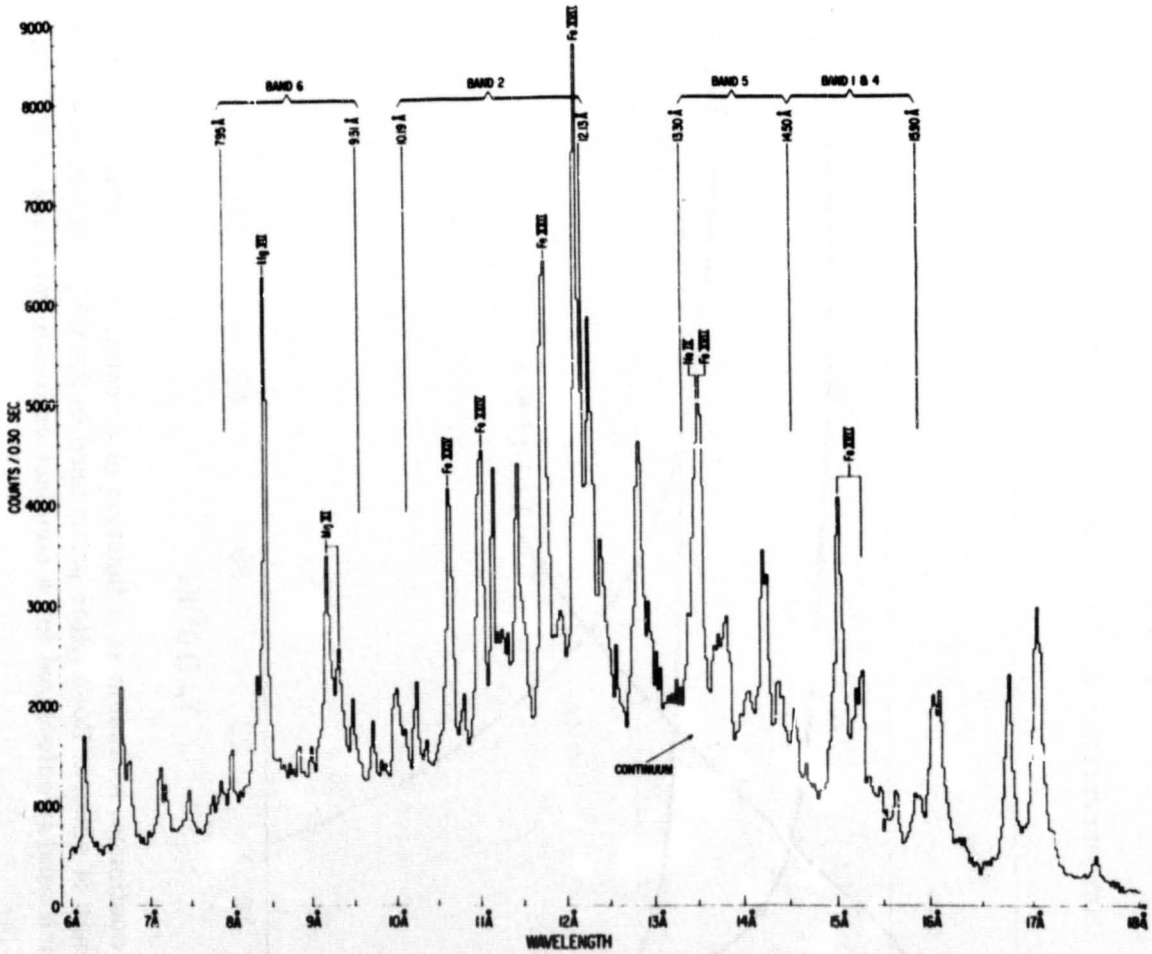

Figure 1. Soft X-ray transmission bands for the Ross filter pairs used in the Long X-ray Spectroheliograph on OSO-7. For illustrative purposes the figure includes the X-ray spectrum of a 2b flare obtained on February 27, 1969, by the Goddard OSO-5 experiment. In most cases, only one or two strong emission lines dominate the bandpass of each filter pair.

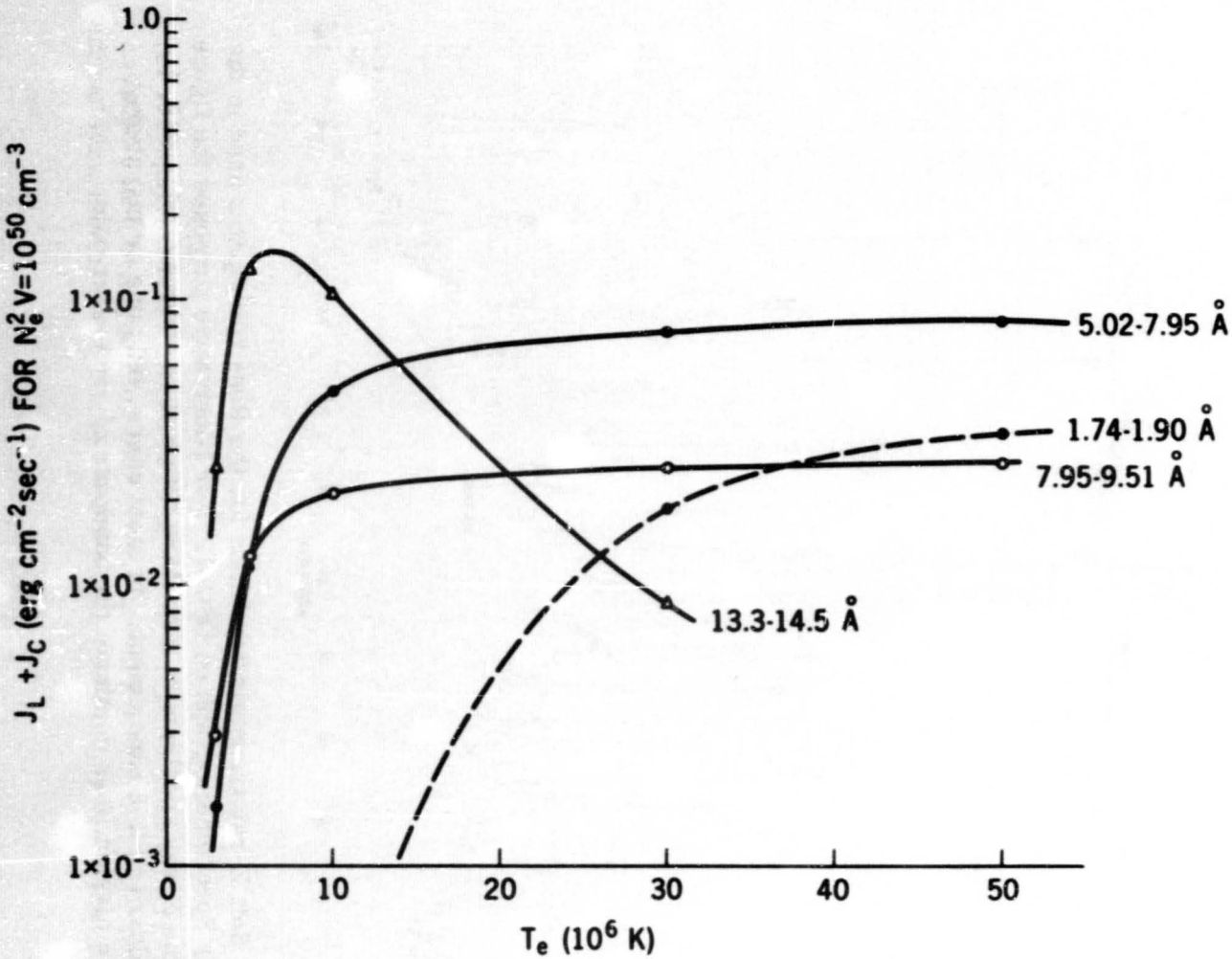

Figure 2. Line and continuum emission as a function of electron temperature integrated over the spectral range of several Ross filter pairs used in the OSO-7 instrument. The incident energy in each band is calculated for a constant emission measure of 10^{50} cm^{-3}.

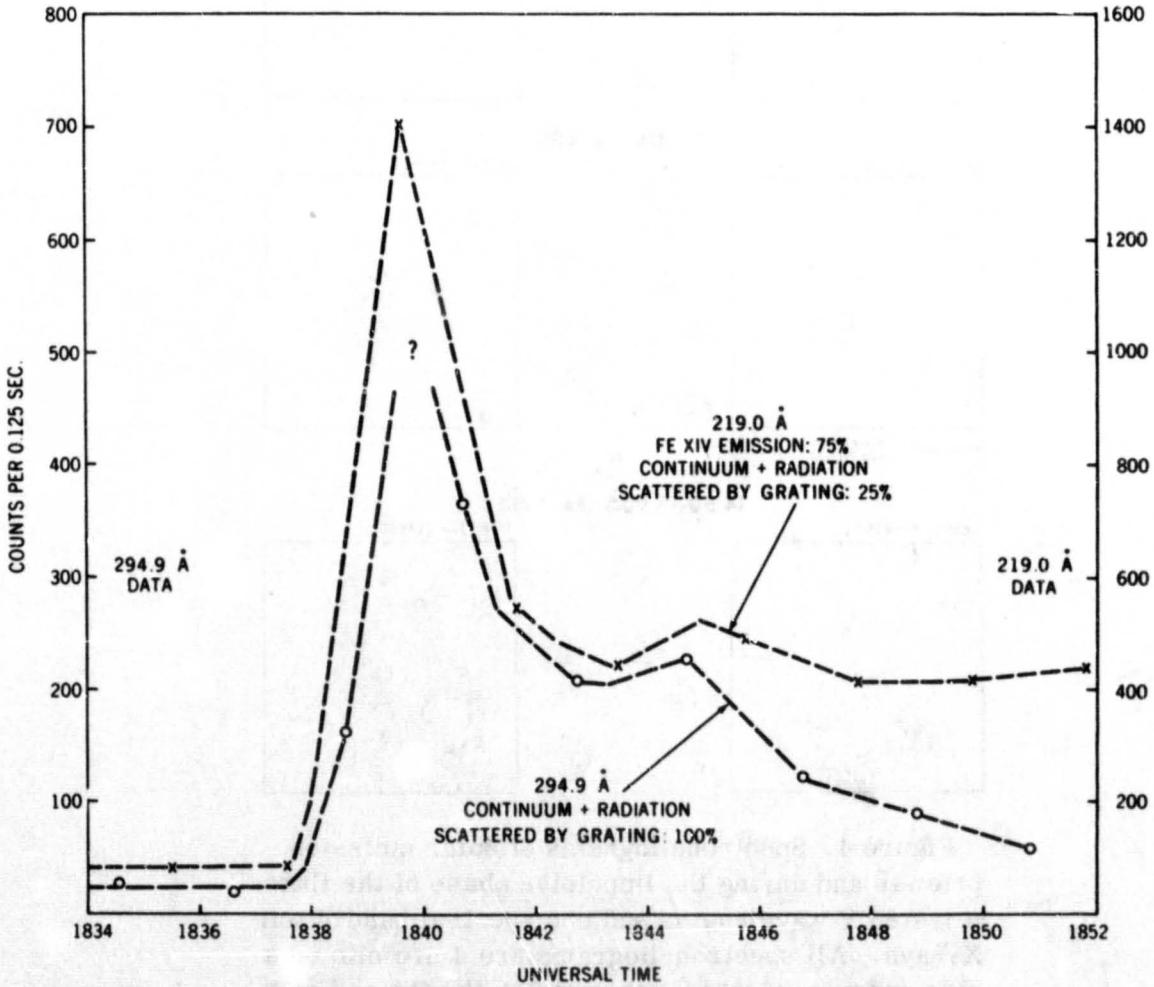

Figure 3. The intensity of the brightest point in the EUV flare of August 2, 1972, at two wavelengths: 219.0Å and 294.9Å. Note the impulsive phase between 1838 and 1842 UT and the gradual phase after 1842 UT seen at both wavelengths.

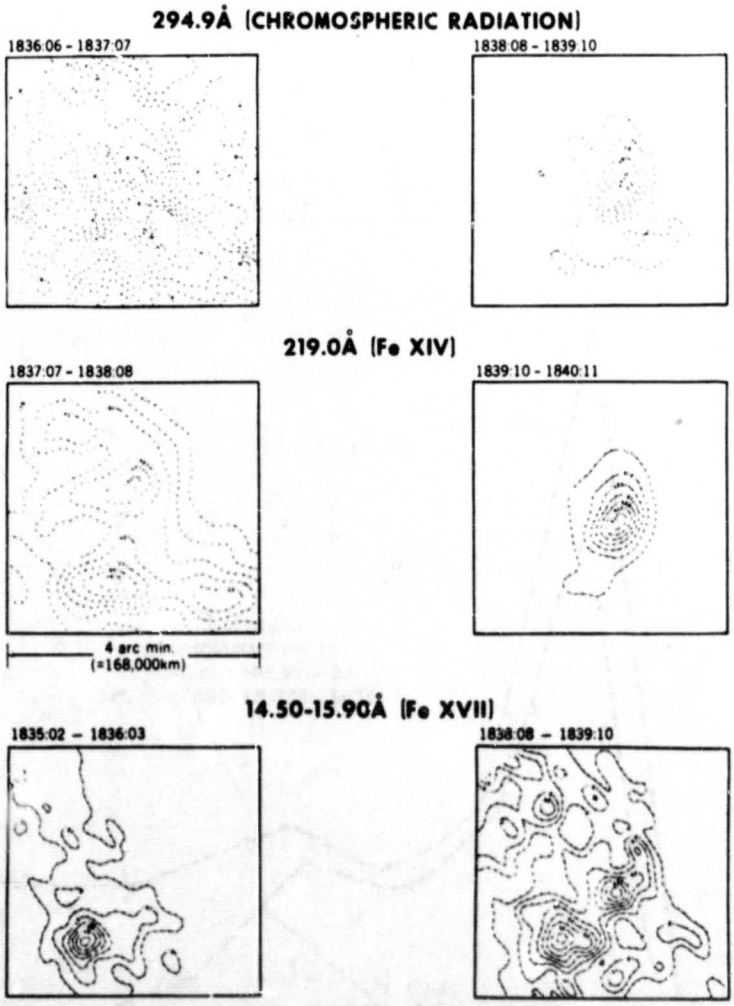

Figure 4. Spectroheliograms of solar emission prior to and during the impulsive phase of the flare at two EUV wavelengths and one spectral band of soft X-rays. All spectroheliograms are 4 arc min on a side and are oriented with north at the top and east to the left. Universal time at the beginning and end of each raster map is shown. Intensity levels have been normalized so that, in each spectroheliogram, the increment between two isophotes represents one-eighth of the maximum intensity found in that spectroheliogram. Note that only weak EUV and no measurable soft X-ray emission emanated from the site of the flare before the event began at 1838 UT. Preflare emission is associated with regions that are bright in Hα.

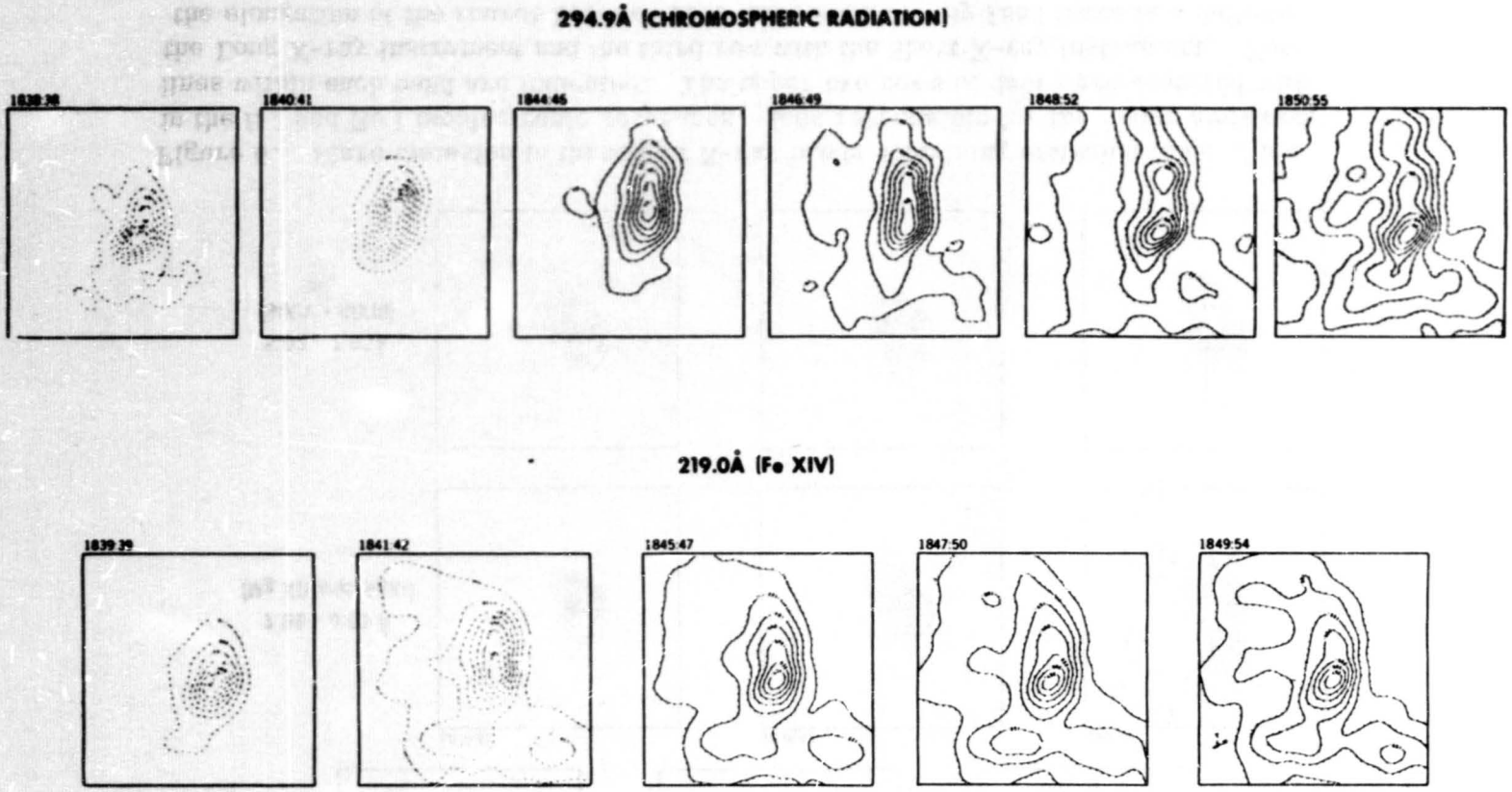

Figure 5. Spatial evolution of EUV flare sources. The earliest frames show the location of the impulsive event at about 1839 UT. Thereafter, the sources become elongated toward the north, but eventually (after 1849) tend to contract again to the initial site of the event. The times indicated on this and following figures refer to the actual time at which the raster scan passed through the center of the flare.

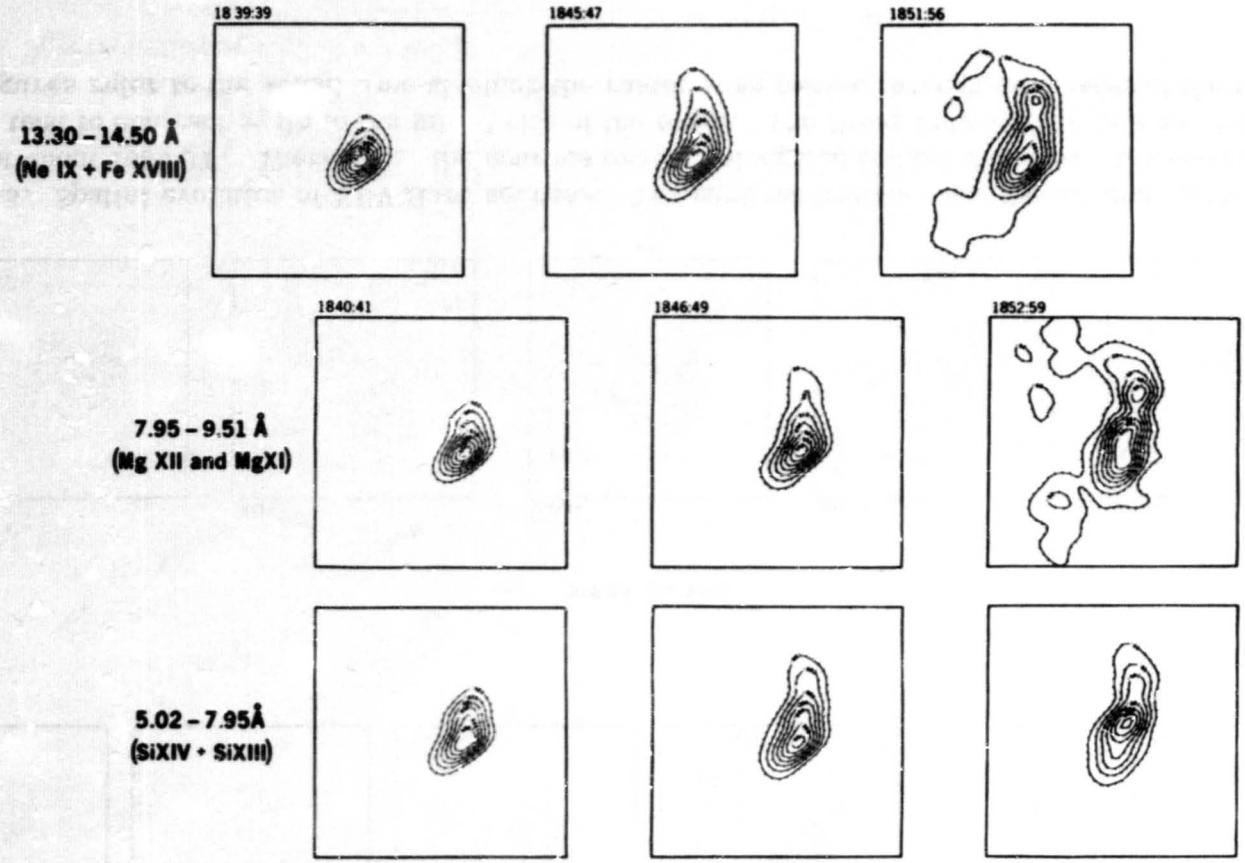

Figure 6. Flare emission in three soft X-ray bands containing emission lines of ions in the H I and He I isoelectronic sequences. Ions responsible for the major emission lines within each band are indicated. The upper two rows of data were acquired with the Long X-ray instrument and the third row with the Short X-ray instrument. Note the elongation of the source between 1839 and 1846 UT. By 1852 there is a definite indication that emission in the 5.02-7.95Å band has shifted toward the location previously occupied by the 1.74-2.07Å source (see next figure).

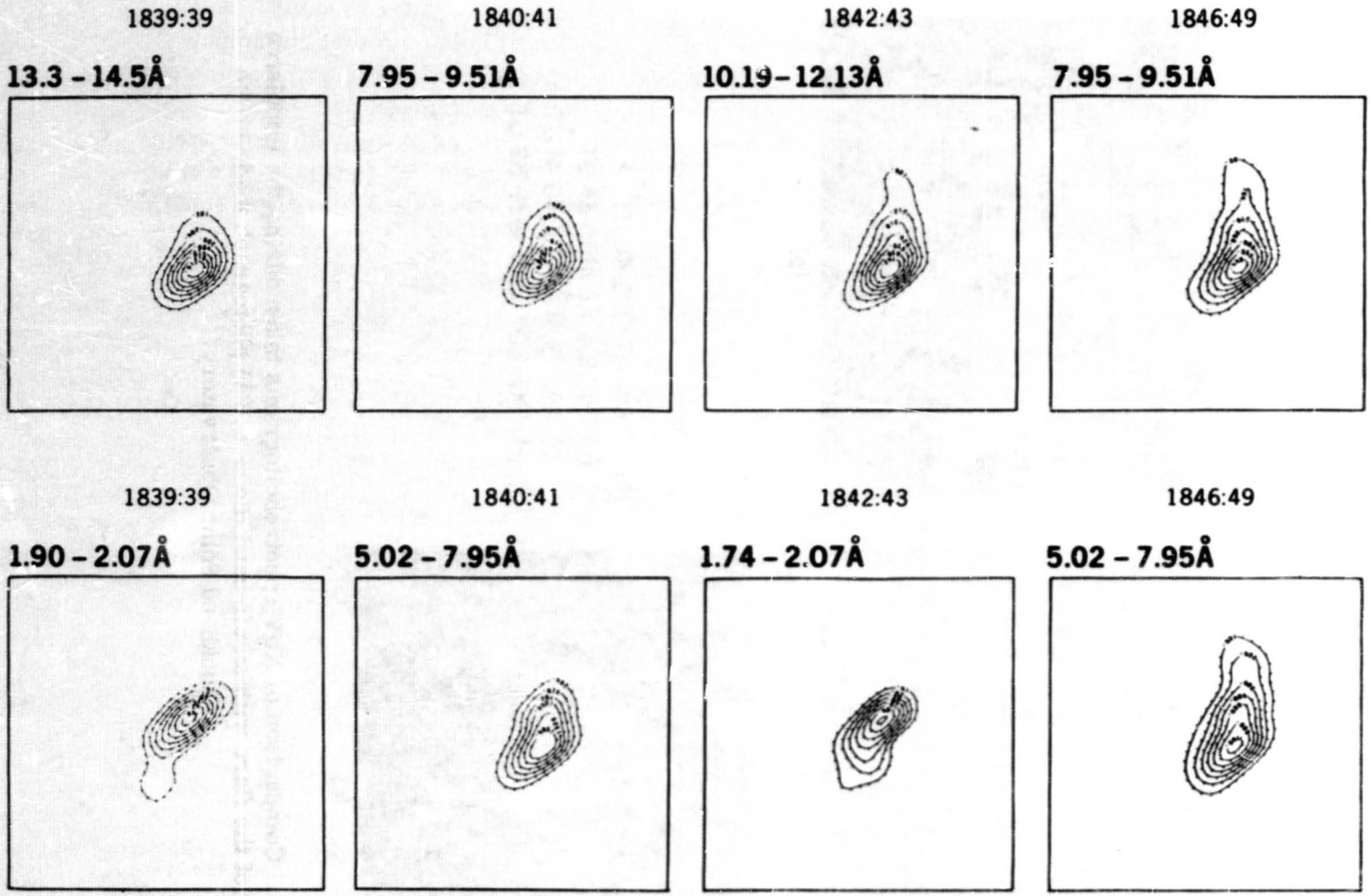

Figure 7. Comparison of soft X-ray spectroheliograms taken concurrently with the Long X-ray and Short X-ray Spectroheliographs. Note that whenever radiation near 1.9Å is being recorded, the source is displaced to the north-east (upper left).

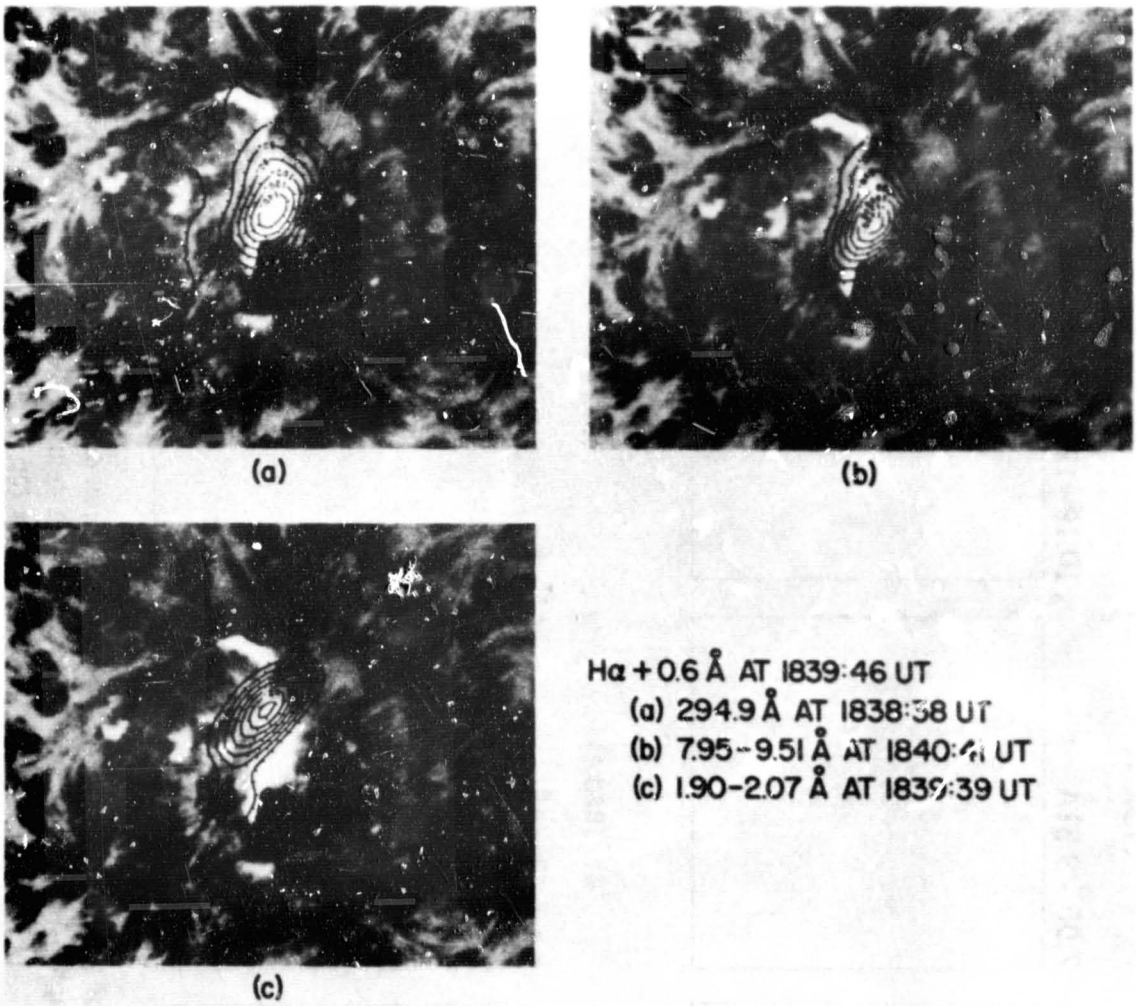

Figure 8. Comparison of XUV spectroheliograms taken during the impulsive phase of the flare with an off-band (Hα + 0.6 Å) photograph made at the Lockheed Solar Observatory.

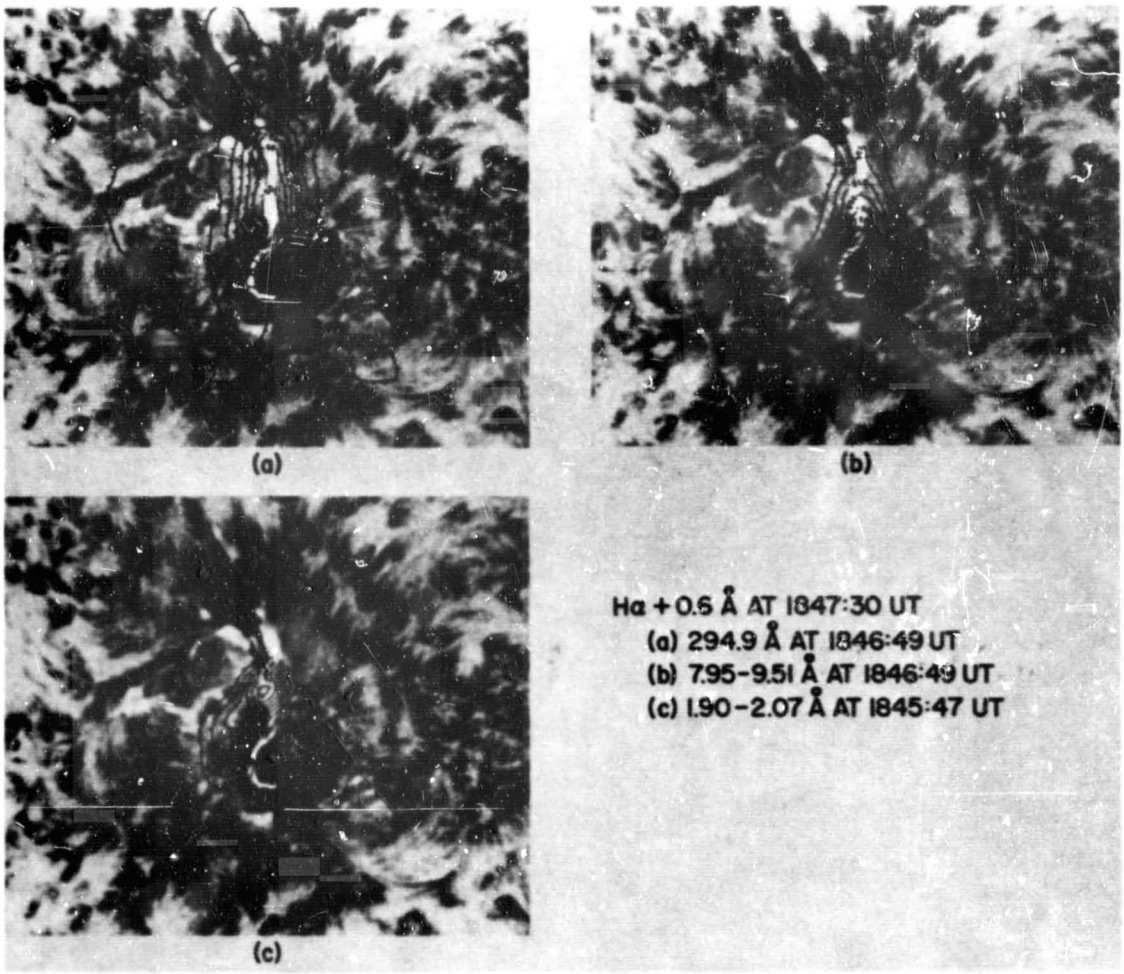

Figure 9. Comparison of the XUV spatial distribution during the post-impulsive phase of the flare with an off-band (Hα + 0.6Å) photograph made at the Lockheed Solar Observatory. The XUV wavelengths are the same as those shown in Figure 8. Note that the radiation at 294.9Å attributed to chromospheric emission coincides with the Hα brightening present at nearly the same time.

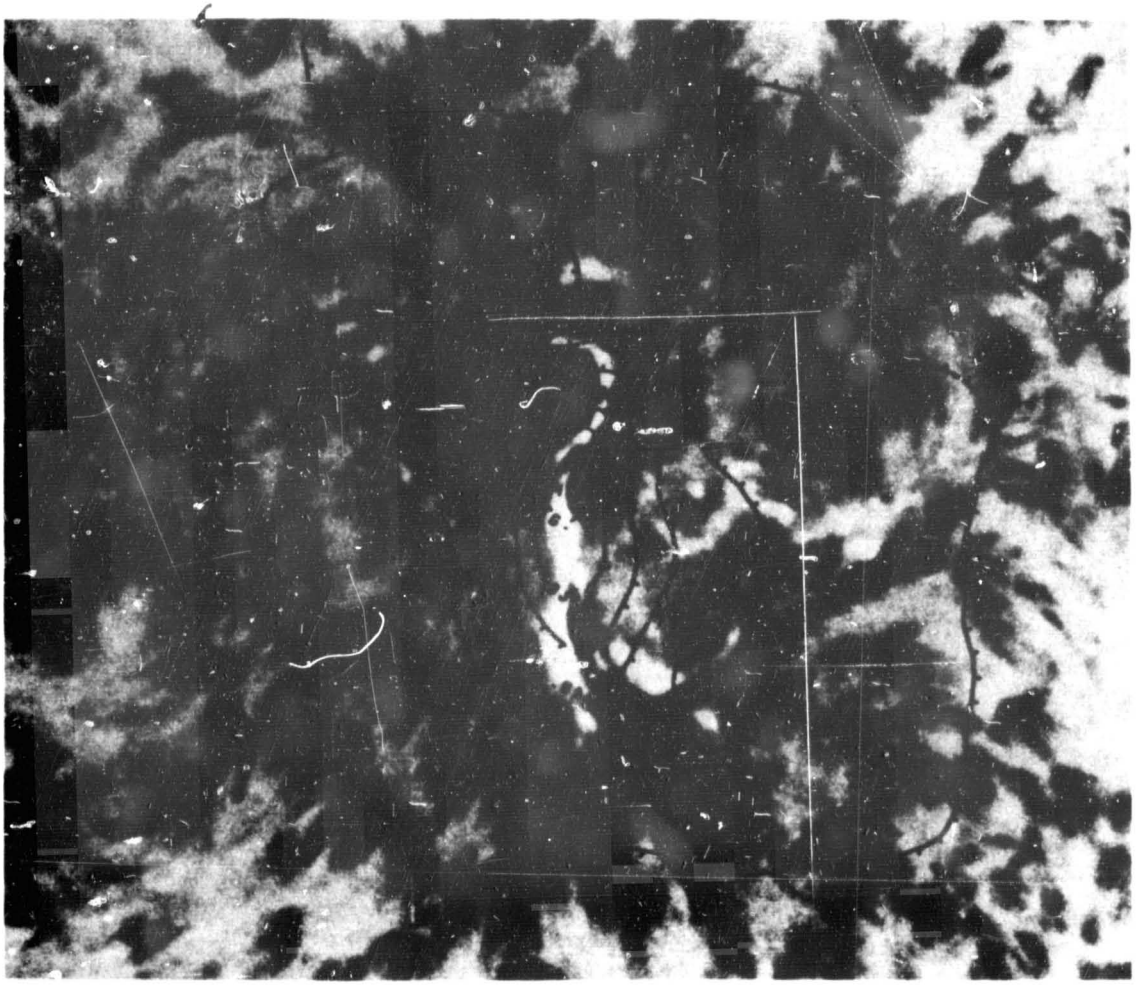

Figure 10. Comparison of an EUV spectroheliogram in the radiation of Fe XIV with an off-band Hα photograph made at the Lockheed Solar Observatory. This ion exhibits the best association with a dark northward-moving surge as shown here at 1847:30 UT. The 219.0Å map was made at 1845:47 UT.

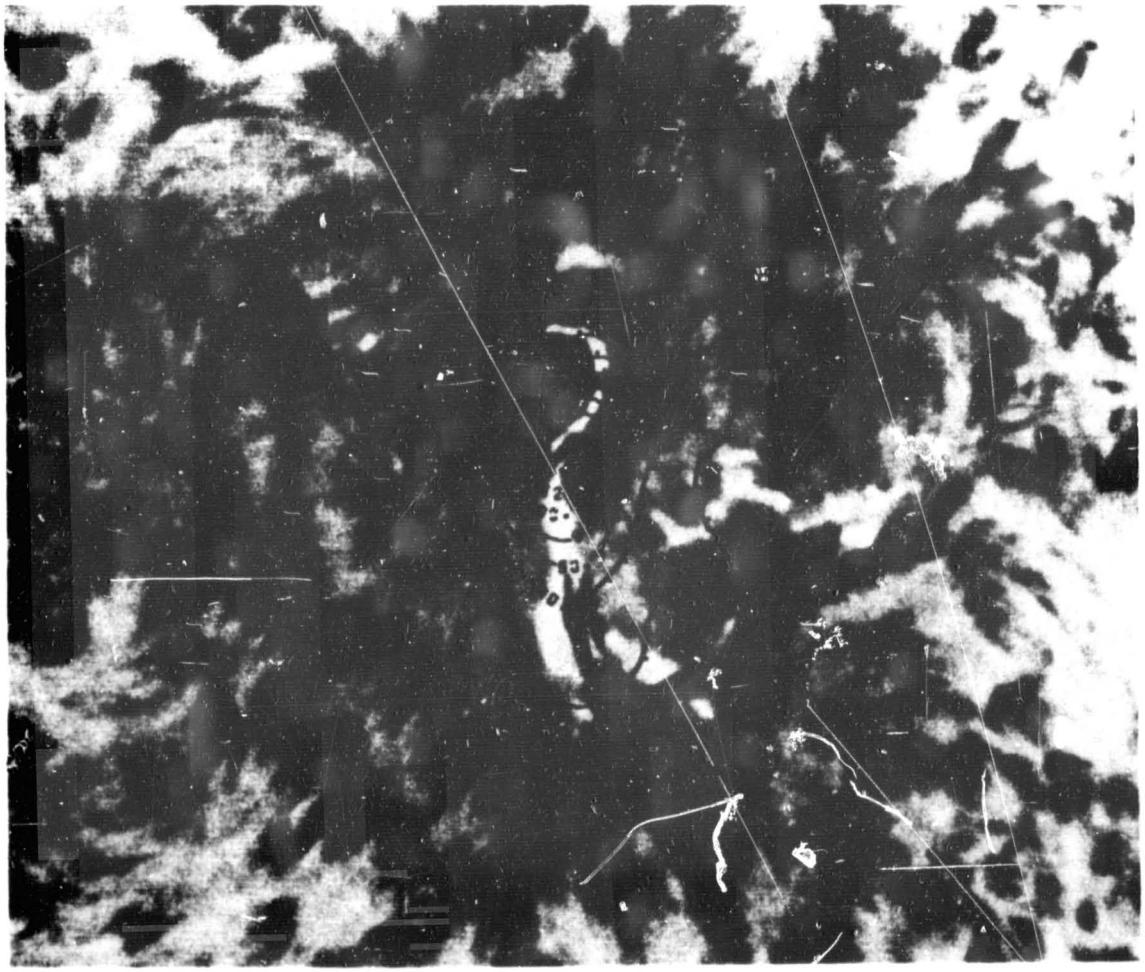

Figure 11. Superposition of an EUV spectroheliogram at 294.9Å taken during the flare's impulsive phase at 1838:38 UT and an off-band Hα photograph recorded as the flare was subsiding at 1847:30 UT. Note that the impulsive EUV radiation originated directly over a dark gap in the bright Hα filament. This gap coincides with the neutral line which separates areas of opposite magnetic polarity in the active region.

☆ U.S. GOVERNMENT PRINTING OFFICE: 1973—734-722/55